Energy Proceedings
Vol 40, 2024
ISSN 2004-2965

Experimental and theoretical study on the NO reduction by H_2 over char decorated with Ni at low temperatures

Kaixuan Feng[1,2], Ruixiang Lin[3], Yuyan Hu[1,2,*], Yuheng Feng[1,2], Dezhen Chen[1,2], Tongcheng Cao[4]

1 Thermal and Environmental Engineering Institute, School of Mechanical Engineering, Tongji University, 1239 Siping Road, Shanghai 200092, China

2 Shanghai Engineering Research Center of Multi-Source Solid Wastes Co-processing and Energy Utilization, 1239 Siping Road, Shanghai 200092, China

3 School of Chemistry, South China Normal University, Guangzhou 510006, China

4 School of Chemical Science and Engineering, Tongji University, 1239 Siping Road, Shanghai 200092, China

(*Corresponding author: yuyan1993@tongji.edu.cn)

ABSTRACT

In this study, we propose a reaction system for the low-temperature reduction of NO by H_2 on carbon-based materials decorated with 5 wt.% Ni. This cost-effective catalyst system efficiently utilizes pyrolysis carbon-based materials and hydrogen. Additionally, it yields environmentally friendly products without requiring extra heat sources in practical SCR process.

Density functional theory elucidates the mechanism of NO heterogeneous reduction by H_2 on Ni-decorated char. Two distinct reaction paths were identified, one involving the intermediate product N_2O and the other not. These pathways exhibit different rate-determination steps and activation energies. Kinetic analysis indicates that the N_2O byproduct pathway has a lower activation energy. Experimental results corroborate the theoretical findings.

Keywords: Char-based catalysis; NO reduction; Low-temperature H_2-Reduction; DFT study;

NONMENCLATURE

Abbreviations	
DFT	Density functional theory
TS	Transition state
Symbols	
ΔE	activation energy

1. INTRODUCTION

Nitrogen oxides (NO_x) are a category of pollutants that pose severe hazards to the environment and human health. They primarily originate from industrial processes, automobile emissions, and activities such as coal combustion. NO_x emissions not only trigger environmental issues like acid rain, photochemical smog, and ozone pollution but are also closely linked to respiratory diseases and cardiovascular problems. Hence, the quest for effective NO_x abatement technologies is of paramount importance for improving environmental quality and safeguarding human health.

Selective Catalytic Reduction (SCR) technology has been widely employed to reduce NO_x emissions. The fundamental principle of SCR involves introducing ammonia (NH_3) or carbon monoxide (CO) from a reducing atmosphere into a reactor, where they react with NO_x, converting it into harmless nitrogen gas (N_2) and water vapor (H_2O). Although SCR technology has achieved some success in NO_x control, it still faces certain challenges. Firstly, NH_3 and CO, as reducing agents, require additional energy input[1], potentially leading to extra energy consumption and environmental impacts. Secondly, the use of NH_3 and CO may result in the emission of nitrogen compounds[2] and carbon oxides[3], adversely affecting atmospheric quality.

To address these issues, our study proposes a novel approach, H_2, as the reducing atmosphere[4], coupled with carbon-based materials loaded with low-cost transition metal nickel (Ni) as active sites—to achieve the low-temperature and highly efficient reduction of NO. Hydrogen energy is a clean energy source with the potential to play a significant role in reducing carbon emissions and achieving sustainable energy supply, while also reducing the need for additional energy in the SCR process[4–8].

This is a paper for 15th International Conference on Applied Energy (ICAE2023), Dec. 3-7, 2023, Doha, Qatar.

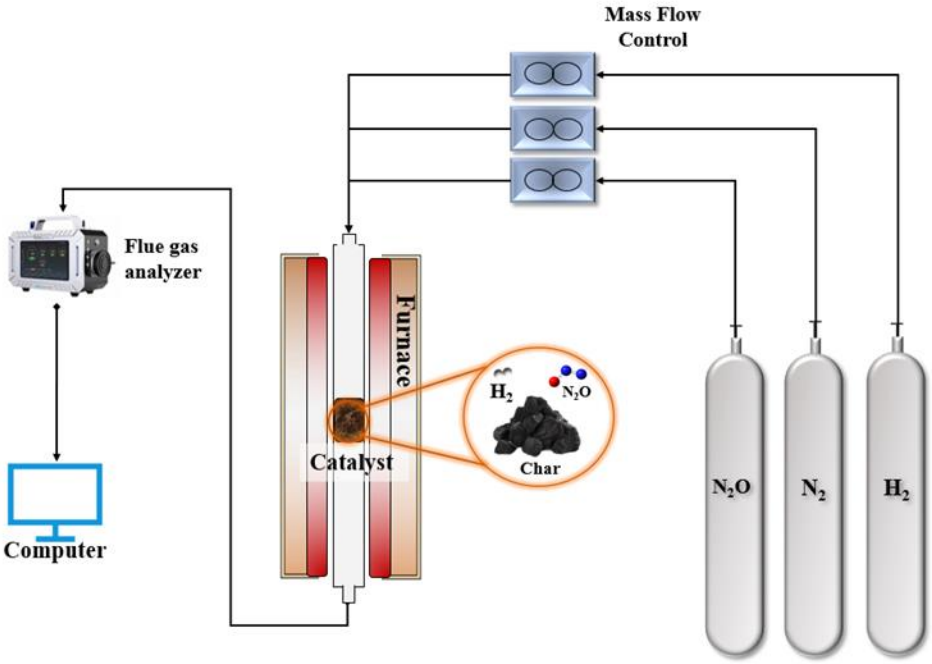

Fig. 1. Experimental device

Our research aims to explore and optimize the SCR technology based on H_2 reduction of NO, providing a more environmentally friendly and efficient solution for reducing NO_x emissions. Additionally, through quantum chemical calculations simulating microscopic reaction mechanisms, we have examined the reaction pathways of NO. By developing this novel catalytic system, we anticipate making significant progress in improving air quality, reducing environmental hazards, and preserving human health.

2. EXPERIMENTAL

2.1 Materials

In this study, commercial charcoal with a particle size ranging from 10 to 24 mesh, obtained from various sources such as wood chips, fruit shells, and coal through processes including carbonization and activation (provided by Aladdin), was used as the raw material. A pure nitric acid reagent was diluted to a 5 wt.% solution, and a total liquid volume of 10 mL/g of the sample was employed for the extraction process. The commercial charcoal was immersed in this solution to eliminate impurities, such as metals and minerals.

Subsequently,m agnetic stirring was carried out at room temperature for two hours, followed by overnight drying at 105 °C.

The charcoal was then cleaned with plasma water until the pH of washing water stabilized at 6-7, effectively removing any excess modifier. Finally, the resulting material was dried for 12 hours at 105 °C in an oven, resulting in the production of the catalyst precursor, which is referred to as "pristine-char."

2.2 Preparations of catalysts

The transition metal-supported char catalyst was prepared by impregnation, using pristine-char as the carrier. In a typical process, a certain amount of metal nitrate was added to deionized water. Subsequently, pristine-char was impregnated with the aqueous solution, with a metal content of 5 wt.%.

The mixture was stirred magnetically at room temperature for 2 hours. Afterward, the mixture was dried for 12 hours at 105°C and then calcined for an additional two hours at 400°C, with a flow rate of 400 mL/min in a nitrogen environment. The calcined sample was then reduced for 2 hours at 250°C, with a flow rate of 250 mL/min of H_2. The resulting catalyst is referred to as Metal-char in this study. To determine the actual metal content on the catalyst, the concentration of transition metals in the solution was measured using an ICP-MS 7700 inductively coupled plasma mass spectrometer (Agilent, USA) and found to be 4.8 wt.

2.3 Experimental system

As depicted in Figure 1, the experimental setup comprises a furnace body, temperature control system, gas distribution system, and a sampling and flue gas analysis system. The furnace body is a vertically oriented tubular electric heating furnace equipped with a PID intelligent temperature control system. Inside the furnace, a metal tube with excellent airtightness,

measuring 270 mm in length and having an inner diameter of 50 mm, serves as the reactor. For each experiment, 2g of catalyst is added and secured using quartz cotton. The total flow rate of the reaction gas is set at 3.2 L/min, with a GHSV (Gas Hourly Space Velocity) of 45,000 h^{-1}.

To maintain precise control, the mass flow of the reaction gas is regulated to achieve gas concentrations of 400 ppm NO and 2000 ppm H_2, while N_2 is introduced as the balance gas during the catalytic activity experiment. The mass flow meter is highly accurate, with a precision of 0.01 sccm. The online recording of outlet NO concentration is performed using the Gasmet Dx4000 analyzer, which offers a rapid response time of 0.001-0.1 seconds and an accuracy of 0.01 ppmv. The catalytic activity is assessed using the NO reduction rate (%), calculated using the following formula:

$$x_{N_2O} = \frac{N_2O_{in} - N_2O_{out}}{N_2O_{in}} \times 100 \quad (1)$$

To eliminate the influence of char adsorption on its catalytic activity evaluation, the sample needs to reach the saturated adsorption of NO before the catalytic reaction begins. During this process, N_2 is used instead of H_2. Once the NO concentration in the outlet flue gas returns to its initial level, H_2 is introduced into the reactor to initiate the catalytic reaction. The NO reduction rate is then recorded once it stabilizes at different temperatures.

2.4 Experimental result

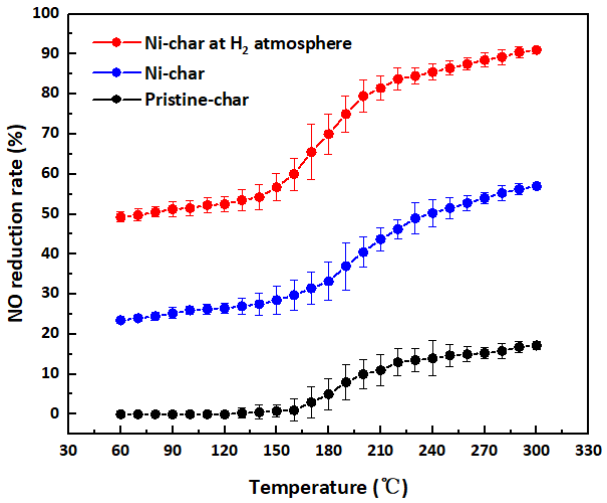

Fig. 2. The reduction rate of NO under different reaction conditions and temperatures

Fig.2 shows the reduction rate of NO under different reaction conditions and temperatures. It is evident that on the pristine-char surface, there is a certain level of NO reduction at a temperature of 200°C, which might be attributed to the inherent reduction capability of the carbon structure itself. However, upon loading Ni as active sites onto the char surface, the NO reduction rate significantly increases. After Ni loading, below 150°C, the catalyst's reduction rate goes from 0% to 20%. Nevertheless, it's worth noting that the catalytic efficiency of Ni active sites is limited.

Between 150°C and 240°C, the reduction rate of NO notably increases to 50%. This could be attributed to an increased reaction rate within this temperature range, where Ni active sites more effectively catalyze the reduction of NO.

When introducing H_2 as a reducing atmosphere, the reduction rate of NO significantly enhances. Below 150°C, the reduction rate increases to 50%, and between 150°C and 240°C, it further escalates to 90%. This indicates that the synergistic effect of H_2 and Ni can substantially promote the reduction of NO.

3. SIMULATION

3.1 Methods

Results should be clear and concise. Density functional theory (DFT) is a widely used method to study the electronic structure of multi-electron systems and surface reaction mechanisms on atomic level. DFT-based functional and basis set of moderate precision is reasonable while calculating both geometry optimization and vibrational frequency. The PEB0 functional[9] and basis set def2-SVP[10] (of double zeta (DZ) quality) have been studied herein to calculate stable configurations of reactants, intermediates, products, and transition states for specific surface reaction processes. For each configuration, information about structural vibrations could be obtained by performing vibrational frequency calculations. To ensure the stability of the structure, there was no imaginary frequency for the reactants, intermediates, and products. To ensure the correctness of the transition states (TSs), there was only one imaginary frequency for each TS, and the corresponding vibrational direction was consistent with the reaction direction. To better describe the dispersion effect, all calculations in the present research were based on the DFT-D3 (BJ)[11] method, which is significantly improved the calculation accuracy and also the most successful and popular one method proposed by Grimme. All calculations were performed using Gaussian16[12].

After obtaining the complete reaction paths, kinetic analyses were carried out. The certain transition states and reactants were thermodynamically analyzed to obtain partition function (with the valley bottom of potential energy surface as the zero point) based on

Shermo[13] during temperatures from 300 to 1000 K, which is within the temperature range of the experiment. The reaction rate constants are calculated by using the TSTcalculator[14] based on eq. 2 and eq. 3.

$$k = \Gamma \times \frac{k_B T}{h} \times \frac{Q_{TS}}{Q_A Q_B} \times \exp(\frac{-E_a}{RT}) \quad (2)$$

$$\Gamma = 1 + \left(\frac{1}{24}\right) \times \left(\frac{h\nu_m c}{k_B T}\right)^2 \quad (3)$$

$$k(T) = A \cdot \exp\left(\frac{-\Delta E}{RT}\right) \quad (4)$$

Here, Γ is the quantum tunneling correction factor (which can be calculated according to eq. 3), k_B is the Boltzmann's constant, T is the reaction temperature, h is the Planck's constant, and Q_{TS}, Q_A, and Q_B are the partition functions of the TS, reactant A, and reactant B, respectively. E_a is the energy barriers for each reaction step, which is identical to the energy difference between the reactant and transition state, and R is the universal gas constant. In eq. 2, ν_m is the imaginary frequency of the transition state, and c is the speed of light.

Then, linear relationship between the natural logarithm of the reaction rate constant (*lnk*) and 1000/T can be obtained, the linear function satisfies Arrhenius equation (eq. 4), where A is the pre-exponential factor and ΔE is the activation energy. As the result, for each elementary reaction, the activation energy, and pre-exponential factor can then be obtained through the intercept and slope in linear relationship.

3.2 Models

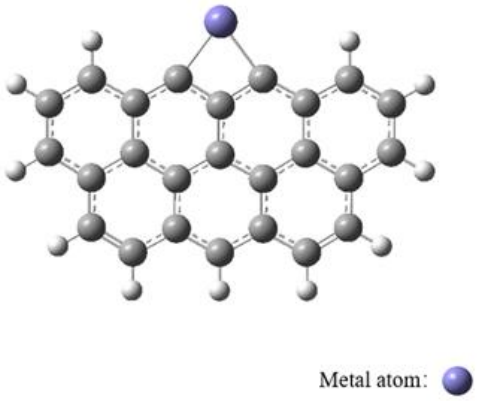

Fig. 3. The model of Ni-char(M)

Char models, with 3 to 7 benzene rings[15] (see Fig. 3), are used for quantum chemical calculations to simulate relevant reaction mechanisms on a char surface, and the results were found consistent with the literatures[16–19]. Fig. 3 shows the char model after being decorated with the transition metal. The purple atom represents the Ni atom which loaded on the middle two C sites [20–23], and the rest C sites on the benzene ring is completely closed by the H atom to simulate the relevant reaction in the hydrogen environment.

3.3 Reaction pathways

3.3.1 The reduction of NO

In Fig. 4, the electrostatic potential[24] of Ni-char is depicted by Multiwfn[25] and VMD[26]. In this representation, blue areas indicate a negative electrostatic potential, while red areas represent a positive electrostatic potential. It is evident from the figure that the electrostatic potential at the Ni sites is notably high.

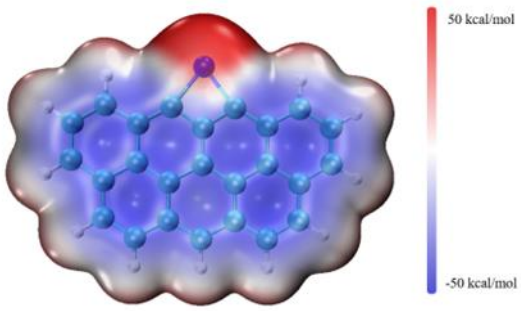

Fig. 4. Electrostatic potential of Ni-char(M)

*During the NO reduction process, it involves two reaction pathways, a*s shown in Fig.5. Considering that in NO molecules, the N atom carries a positive charge, and the O atom carries a negative charge, NO tends to preferentially adsorb in an "O-down" mode on the Ni sites. This results in the formation of the M1 structure and release the energy of 41.1 kJ/mol.

Next, the second NO molecule similarly adsorbs onto the Ni site in an "O-down" mode, forming the M2 structure. At this point, a substantial amount of energy, 283.5 kJ/mol, is released. This is attributed not only to the adsorption of the second NO molecule but also to the formation of stable chemical bonds between the N1 and N2 atoms within the M2 structure, thereby strengthening the interactions between the two O atoms and the Ni atom.

Subsequently, the reduction process of NO takes place, where the stable M2 structure surpasses a transition state TS1 with an energy barrier of 100.8 kJ/mol. At this stage, two products emerge (1M3 and 2M3), leading to the differentiation of NO reduction into distinct reaction pathways (reaction 1 and reaction 2).

The spin states differ between the 1M3 and 2M3 structures, with a spin of 2 for the 1M3 structure and a spin of 4 for the 2M3 structure. A lower spin state leads to increased stability of the electronic system.

Consequently, in the structure, a noticeable bonding occurs between O1 and Ni atoms, resulting in the entire system lying in the same plane.

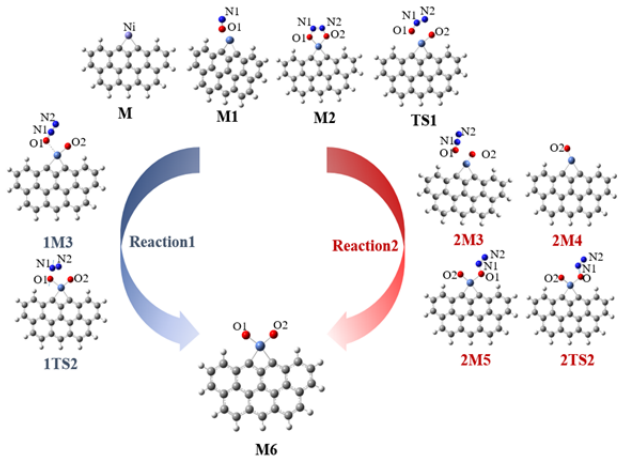

Fig. 5. Two reaction pathways involved in NO reduction process

In the 2M3 structure, the higher spin state contributes to relative instability in the configuration. The O1-N2 bond breaks and there is a noticeable dihedral angle between O1-N1-N2 and Ni-char, causing them not to lie in the same plane. As a result, the relative energy of the 2M3 structure is higher than that of the 1M3 structure (-225.6 kJ/mol vs. -254.1 kJ/mol). Table 1 shows the Mayer bond levels[27] between some important atoms. The bond between O1 and Ni weakens noticeably, and the interaction between the O1 and N1 atom is stronger.

Table.1. Mayer bond levels between some important atoms

Mayer bond	1M3	2M3
Ni-O1	0.09	0.05
Ni-O2	0.46	0.35
O1-N1	0.77	1.00
N1-N2	1.13	1.14

In order to guess the next reaction process, flexible scanning was performed on the 1M3 and 2M3 structures to record the total energy change of the system as the number of O1-Ni atoms gradually increased, as shown in the Fig. 6.

During the scanning process, it can be observed that the 1M3 and 2M3 structures exhibit significantly contrasting trends in energy changes. As the N2-N1-O1 fragment dissociates, the energy of the 1M3 structure steadily increases, indicating that the 1M3 structure cannot spontaneously dissociate from N_2O.

Therefore, for the 1M3 structure, the next step in the reaction can only involve the removal of N_2, leading directly to the formation of the M6 structure. The 1M3 structure subsequently absorbs a significant amount of heat (170.6 kJ/mol) to cross the second transition state, 1TS2. This process results in the release of N_2 and the formation of product M6, with both O atoms remaining on the catalyst's surface, which indicates that the reduction of NO leads to the oxidation of Ni atoms.

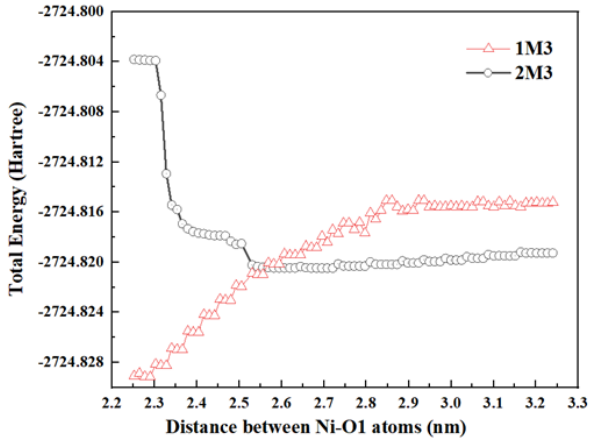

Fig. 6. Flexible Scanning the length of N1-O1 Bond in 1M2 and 2M2

In contrast, for the 2M3 structure, the energy exhibits a sudden decrease, followed by a subtle rise with minor fluctuations. The slight energy increase may be associated with weak interactions between the O atom and hydrogen atoms on the C structure. Flexible scans further confirm the strong propensity of the 2M3 structure for the direct dissociation of the N_2O fragment, aligning well with experimental observations[28,29]. N_2O can be released independently during this process. Flexible scanning confirms the self-release of N_2O. Following this, N_2O re-adsorbs onto the catalyst's surface in an "O-down" fashion to form the 2M4 structure. This structure requires crossing a transition state of only 26.3 kJ/mol to complete the release of N_2 and generate product M6.

Reaction 2 generates an intermediate product, N_2O, during the reduction of NO. Subsequently, it undergoes the reduction of N_2O, and N_2O is readmitted to the Ni site to form 2M5. This structure is similar to 1M2 and 2M2 structures but possesses lower energy. In Fig.7, we present the weak interactions[30] of 1M2, 2M2, and 2M5. It can be observed that the interaction between O1 and Ni atoms in the 2M5 structure is the strongest, forming a stable chemical bond, which is absent in the 1M2 and 2M2 structures. Due to the strong interaction between O1 and Ni, the Mayer bond order between O1 and Ni is weakened, requiring few amount of energy to release the N_2 molecule.

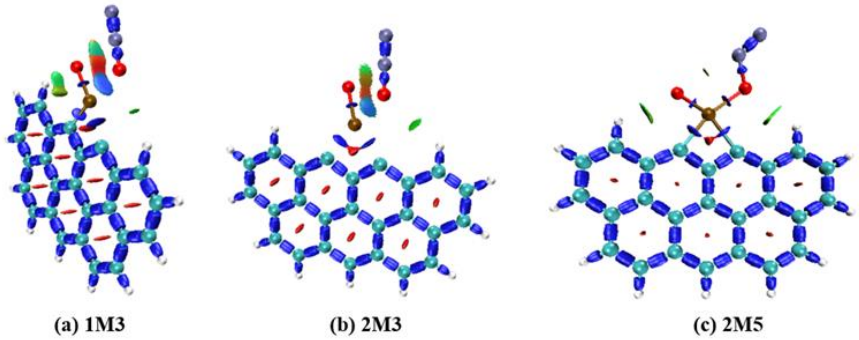

Fig. 7. Weak interaction analysis in 1M3, 2M3, 2M5

The potential energy surface during the reaction process, depicting the relative energy of reactants, transition states, and products, is illustrated in the Fig 8.

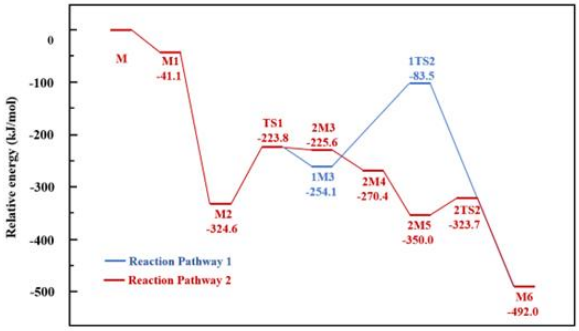

Fig. 8. Potential energy surface during NO reduction process

3.3.2 The generation of H_2O

At this stage, both Reaction 1 and Reaction 2 have resulted in the formation of the M6 structure. This is due to the reducing atmosphere of H_2, where free hydrogen atoms adsorb onto two oxygen sites, creating the M7 structure (see in Fig.9). Subsequently, M7 undergoes a transition state where a hydrogen atom transfers from one oxygen atom to another, leading to the formation of H_2O molecules that escape. As a result, the char surface retains only one oxygen atom, allowing the reaction to continue.

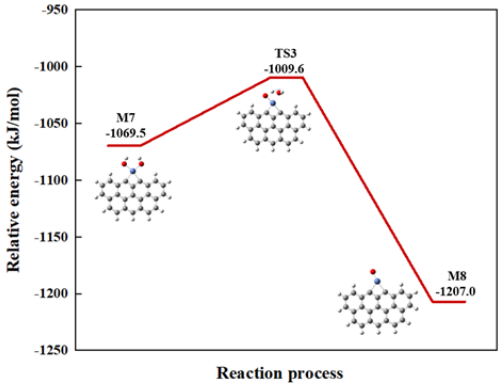

Fig. 9. Potential energy surface during H2O generation process

3.4 Kinetic characteristics

After calculating the complete reaction path, we conduct kinetic analysis for each reaction pathway to obtain the activation energy and pre-exponential factor. For the reaction pathways of NO reduction by H_2 on pristine-char and transition metal decorated char, the rate-determining step is selected respectively.

The step of (1M3→1TS2→P) is the rate-determining step in reaction pathway 1. The step of (M2→TS1→2M3) is the rate-determining step in reaction pathway 2.

Several steps are taken for the rate-determination steps in various reaction processes, including (1) selecting the reactants and transition state structures in the rate-determination steps, (2) calculating the partition function at different temperatures based on Shermo[13], and (3) obtaining the reaction rate K at different temperature points through TST calculator based on formulas (1) and (2). The linear relationship between the natural logarithm of the reaction rate constant(lnk) and 1000/T can be obtained, as shown in Fig. 10. The linear function satisfies the Arrhenius equation (Eq. 3), where A is the pre-exponential factor, ΔE is the activation energy. As a result, the activation energy and pre-exponential factor can be obtained from the intercept and slope of the linear relationship for each rate-determination step, given in Table 2.

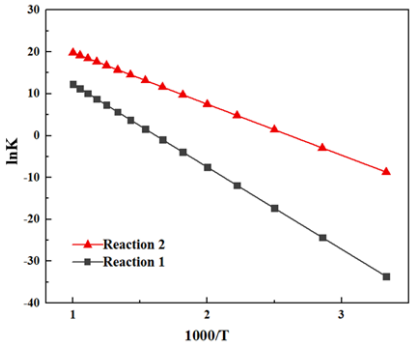

Fig. 10. Calculated rate constants in the temperature range 300 K~1000 K

Table.2. Kinetic parameters for the Arrhenius expression of the rate-determining steps

	Reaction1	Reaction2
Activation Energy, Ea (kJ·mol^{-1})	163.7	101.8
Pre-exponential factor, A (s^{-1})	7.26E+13	8.23E+13

From Fig.10 and Table 2, it is evident that the reaction2 exhibits a higher reaction rate, lower activation energy (101.8kJ/mol vs. 163.7 kJ/mol), and a higher pre-exponential factor (8.23E+13 vs. 7.26E+13). This indicates that during the reduction of NO, there is a preference for the formation of intermediate product N2O. However, it is important to note that in experiments and numerous literature sources, the accumulation of N_2O during the NO reduction process has not been observed. This is because the consumption rate of N_2O is significantly faster than its production rate. Theoretically, we have found that the reduction of N2O to N_2 only requires overcoming an energy barrier of 26.3 kJ/mol, whereas the formation of N_2O requires an energy barrier of 100.8 kJ/mol. According to some experimental data[28,29], the content of N_2O will at first increase in the denitration process, and then rapidly become decomposed. The here presented simulated results is consistent with these experimental observations.

4. CONCLUSION

In this study, we have successfully demonstrated that carbon-based materials loaded with nickel (Ni) catalysts, in the presence of hydrogen gas (H_2), effectively catalyze the reduction of nitrogen oxides (NO_x). Our experimental results highlight the promising applications of this catalytic system, allowing for the efficient utilization of waste hydrogen and discarded carbon materials. Notably, this system operates at low reaction temperatures and offers cost-effective advantages while producing environmentally friendly byproducts.

During the course of these reactions, we have identified two distinct reaction pathways. Although the reduction of NO can proceed through various routes, our research indicates a pronounced preference for the reduction of NO into nitrous oxide (N_2O). This finding is of paramount importance for understanding the reaction mechanisms and optimizing the catalytic process. These pathways exhibit varying activation energies, with one pathway leading to the formation of N_2O as an intermediate product, while the other does not. Consequently, our results strongly suggest that the reduction of NO is inclined towards the generation of the intermediate N_2O, offering valuable insights for further process optimization and control.

In summary, the outcomes of this study provide a novel theoretical and experimental foundation for the design and application of carbon-based materials loaded with Ni catalysts. These findings hold great promise for making substantial contributions to environmental protection and resource utilization. Future research endeavors can delve deeper into elucidating reaction mechanisms to enhance catalytic efficiency and selectivity, thus better aligning with the needs of both industrial and environmental sectors.

ACKNOWLEDGEMENT

The study was financially supported by National Key R&D Program of China (grant number: 2018YFD1100600).

The authors declare that they have no known competing financial interests or personal relationships that could have appeared to influence the work reported in this paper.

DECLARATION OF INTEREST STATEMENT

The authors declare that they have no known competing financial interests or personal relationships that could have appeared to influence the work reported in this paper. All authors read and approved the final manuscript.

REFERENCE

[1] Van der Geer J, Hanraads JAJ, Lupton RA. The art of writing a scientific article. J Sci Commun 2010;163:51–9. (Reference to a journal publication)

[2] Strunk Jr W, White EB. The elements of style. 4th ed. New York: Longman; 2000. (Reference to a book)

[3] Mettam GR, Adams LB. How to prepare an electronic version of your article. In: Jones BS, Smith RZ, editors. Introduction to the electronic age, New York: E-Publishing Inc; 2009, p. 281–304. (Reference to a chapter in an edited book)

[4] Mitchell, J.A., Thomson, M., & Coyne, R.P. (2017, January 25) APA citation. *How and when to reference*. Retrieved from https://www.howandwhentoreference.com/APAcitation

[1] Shen B, Chen J, Yue S, et al. A comparative study of modified cotton biochar and activated carbon based catalysts in low temperature SCR. Fuel 156, 47–53 (2015).

[2] Wang D, Yao Q, Mou C, et al. New insight into N_2O

formation from NH3 oxidation over MnO /TiO_2 catalyst. Fuel 254, 115719 (2019).
[3] Nobukawa T, Yoshida M, Okumura K, et al. Effect of reductants in N_2O reduction over Fe-MFI catalysts. Journal of Catalysis 229, 374–388 (2005).
[4] Guan Y, Liu Y, Lv Q, et al. Review on the selective catalytic reduction of NO with H_2 by using novel catalysts. Journal of Environmental Chemical Engineering 9, 106770 (2021).
[5] Jong KG, Hun SJ, Bin KS, et al. The role of Pt valence state and La doping on titanium supported Pt-La/TiO_2 catalyst for selective catalytic reduction with H_2. Applied Surface Science 608, 155040 (2023).
[6] Cheng X, Su D, Wang Z, et al. Catalytic reduction of nitrogen oxide by carbon monoxide, methane and hydrogen over transition metals supported on BEA zeolites. International Journal of Hydrogen Energy 43, 21969–21981 (2018).
[7] Castoldi L, Matarrese R, Liu C, et al. Dynamics and Selectivity of N_2O Formation/Reduction During Regeneration Phase of Pt-Based Catalysts. Top Catal 61, 1672–1683 (2018).
[8] Hu Z, Yang, RT. 110th Anniversary: Recent Progress and Future Challenges in Selective Catalytic Reduction of NO by H2 in the Presence of O2. Ind. Eng. Chem. Res. 58, 10140–10153 (2019).
[9] Adamo C, Barone V. Toward reliable density functional methods without adjustable parameters: The PBE0 model. The Journal of Chemical Physics 110, 6158–6170 (1999).
[10] Weigend F, Ahlrichs R. Balanced basis sets of split valence, triple zeta valence and quadruple zeta valence quality for H to Rn: Design and assessment of accuracy. Phys. Chem. Chem. Phys. 7, 3297 (2005).
[11] Bursch M, Eike C, Andreas H, et al. Understanding and Quantifying London Dispersion Effects in Organometallic Complexes. Acc. Chem. Res. 52, 258–266 (2019).
[12] Frisch MJ, Trucks GW, Schlegel HB, et al. Gaussian. (2016)
[13] Lu T, Chen Q. Shermo: A general code for calculating molecular thermochemistry properties. Computational and Theoretical Chemistry 1200, 113249 (2021).
[14] Tian, L. TSTcalculator. Gaussian 16; Gaussian, Inc.: Wallingford, CT, 2016.
[15] Perry ST, Hambly EM, Fletcher TH, et al. Solid-state 13C NMR characterization of matched tars and chars from rapid coal devolatilization. Proceedings of the Combustion Institute 28, 2313–2319 (2000).
[16] Zhang XX, Xie M, Wu H, Lv X, et al. DFT study of the effect of Ca on NO heterogeneous reduction by char. Fuel 265, (2020).
[17] Zhang XX, Xie M, Wu HX, et al. Microscopic effect mechanism of Ca on NO heterogeneous reduction by char: A DFT study. Journal of Fuel Chemistry and Technology 48, 163–171 (2020).
[18] Li Y, Niu SL, Lu CM, et al. Molecular simulation study of NO heterogeneous reduction by biomass reburning. Journal of Fuel Chemistry and Technology 48, 689–697 (2020).
[19] Chen P, Gu M, Chen X, et al. Study of the reaction mechanism of oxygen to heterogeneous reduction of NO by char. Fuel 236, 1213–1225 (2019).
[20] Feng KX, Hu YY, Cao TC. Effect of K-decoration on the generation and reduction of N_2O onto a biochar surface. Fuel 316, 123148 (2022).
[21] Feng KX, Hu YY, Cao TC. Mechanism of Fuel Gas Denitration on the KOH-Activated Biochar Surface. J. Phys. Chem. A 126, 296–305 (2022).
[22] Zhang XX, Xie M, Wu H, et al. DFT study of the effect of Ca on NO heterogeneous reduction by char. Fuel 265, 116995 (2020).
[23] Yang JC. Chen L, Su JC, et al. Mechanism on the effect of sodium on the heterogeneous reduction reaction of NO by Char(N). Fuel 321, 124065 (2022).
[24] Murray JS, Politzer P. The electrostatic potential: an overview. Wiley Interdiscip Rev: Comput Mol Sci 2011;1(2):153–63
[25] Lu T, Chen, FW. Multiwfn: A multifunctional wave function analyzer. J. Comput. Chem. 33, 580–592 (2012).
[26] Humphrey W, Dalke A, Schulten K. VMD: Visual molecular dynamics. Journal of Molecular Graphics 14, 33–38 (1996).
[27] Mayer, I. Bond orders and valences from ab initio wave functions. Int. J. Quantum Chem. 29, 477–483 (1986).
[28] Li QY, Hou YQ, Wang JC et al. Superiority of Raw Biomass and Potassium Hydroxide in Preparation of Ultrahigh Nitrogen Doping of Carbon for NH_3-SCR Reaction. ACS Sustainable Chem. Eng. 8, 11308–11316 (2020).
[29] Chen, H. Using Activated Char from Sewage Sludge Pyrolysis and Hydrazine for flue Gas denitration: Performance and Mechanism Investigation. (Tongji University, 2017).
[30] Lu T, Chen Q. Interaction region indicator (IRI): A very simple real space function clearly revealing both chemical bonds and weak interactions.